PCCP

PAPER

View Article Online
View Journal | View Issue

Cite this: *Phys. Chem. Chem. Phys.*, 2015, **17**, 3214

Molecular dynamics simulation of spin–lattice NMR relaxation in poly-L-lysine dendrimers: manifestation of the semiflexibility effect

Denis A. Markelov,*[a] Stanislav G. Falkovich,[b] Igor M. Neelov,[bc] Maxim Yu. Ilyash,[b] Vladimir V. Matveev,[a] Erkki Lähderanta,[d] Petri Ingman[e] and Anatolii A. Darinskii[bc]

Received 22nd October 2014,
Accepted 8th December 2014

DOI: 10.1039/c4cp04825c

www.rsc.org/pccp

NMR relaxation experiments are widely used to investigate the local orientation mobility in dendrimers. In particular, the NMR method allows one to measure the spin–lattice relaxation rate, $1/T_1$, which is connected with the orientational autocorrelation function (ACF) of NMR active groups. We calculate the temperature (Θ) and frequency (ω) dependences of the spin–lattice NMR relaxation rates for segments and NMR active CH_2 groups in poly-L-lysine (PLL) dendrimers in water, on the basis of full-atomic molecular dynamics simulations. It is shown that the position of the maximum of $1/T_1(\omega)$ depends on the location of the segments inside the dendrimer. This dependence of the maximum is explained by the restricted flexibility of the dendrimer. Such behavior has been predicted recently by the analytical theory based on the semi-flexible viscoelastic model. The simulated temperature dependences of $1/T_1$ for terminal and inner groups in PLL dendrimers of n = 2 and n = 4 generations dissolved in water are in good agreement with the NMR experimental data, which have been obtained for these systems previously by us. It is shown that in the case of PLL dendrimers, the traditional procedure of the interpretation of NMR experimental data – when smaller values of $1/T_1$ correspond to higher orientation mobility – is applicable to the whole accessible frequency interval only for the terminal groups. For the inner groups, this procedure is valid only at low frequencies.

I. Introduction

Dendrimers are perfect, tree-like macromolecules with a well-controlled chemical structure, which have been synthesized more than 30 years ago.[1–5] Due to their spherical symmetry and compactness, on the one hand, and their softness, on the other, they are intermediate entities between colloids and linear polymers. They can be used in various industrial applications, such as biomedicine,[6–10] energy harvesting,[11–13] catalysis,[14,15] and other fields.[16–18]

The relaxation properties of dendrimers are of considerable importance in many practical applications.[19–23] Even for a single dendrimer macromolecule, there are many relaxation processes with different lengths and time scales, starting from the rotation as a whole to the local segmental mobility. Different experimental methods are used to describe distinctive features of dendrimers (see *e.g.* ref. 24–26).

NMR relaxation experiments are widely used to study local orientation mobility in dendrimers.[27–38] In particular, the NMR method allows one to measure the spin–lattice relaxation rate, $1/T_1$, which is connected with the orientational autocorrelation function (ACF) of NMR active groups.

The traditional approach to estimate the mobility of NMR active groups is the measurement of $1/T_1$ at a fixed temperature and frequency.[13,27–29] In this approach, the lower $1/T_1$ value corresponds to the higher mobility. However, Pinto *et al.*[37] have shown that the application of this approach can lead to mis-interpretations. It has been experimentally established for poly(aryl ether) dendrimers that a direct correlation exists only between the spin–spin relaxation time (T_2), or the nuclear Overhauser effect (NOE), and the mobility of the NMR active groups. These characteristics have a monotonic dependence on the layer number in the dendrimer. However, $1/T_1$ has a non-monotonic layer number dependence at room temperature. The reason for this behavior is the fact that the dependence of $1/T_1$ on a reciprocal temperature has a maximum.[39]

[a] *Faculty of Physics, St. Petersburg State University, Ulyanovskaya Str. 1, Petrodvorets, St. Petersburg, 198504 Russia. E-mail: markeloved@gmail.com*
[b] *Institute of Macromolecular Compounds, Russian Academy of Sciences, Bolshoi Prospect 31, V.O., St. Petersburg, 199004 Russia. E-mail: a.darinskii@mail.ru*
[c] *St. Petersburg National Research University of Information Technologies, Mechanics and Optics (ITMO University), Kronverkskiy pr. 49, St. Petersburg, 197101, Russia. E-mail: i.neelov@mail.ru*
[d] *Laboratory of Physics, Lappeenranta University of Technology, Box 20, 53851 Lappeenranta, Finland. E-mail: erkki.lahderanta@lut.fi*
[e] *Instrument Centre, Department of Chemistry, University of Turku, Vatselankatu 2, FI-20014, Turku, Finland. E-mail: pingman@utu.fi*

Therefore, the mentioned procedure can be applied only when the measured $1/T_1$ values are located on the left side of the maximum. In particular, this situation is realized in solutions of linear polymers. However, for dendrimers the position of the measured $1/T_1$ values with respect to the maximum can depend on the chemical structure of the dendrimer and on the location of the NMR active groups inside the dendrimer. As reported for poly(aryl ether),[37] the non-monotonic behavior takes place due to the fact that the values of $1/T_1$, measured for different layers correspond to different sides of the temperature dependence with respect to the maximum. Similar behavior was observed for other dendrimers, as well.[32,35,36] Therefore, for the correct interpretation of the $1/T_1$ data of dendrimers, the temperature dependence of $1/T_1$ is necessary.

Although there are many experimental studies on the NMR relaxation in dendrimers, the number of theoretical investigations in this field is insufficient. As a rule, the theory considers the frequency dependence of $1/T_1$ at a constant temperature in contrast to the NMR experiments, where the temperature dependence at a fixed frequency, ω, is studied. In this case, the maximum is observed on the frequency dependence of the reduced spin–lattice relaxation rate of ^{1}H atoms:

$$\left[\frac{1}{T_{1\mathrm{H}}}(\omega)\right] = \frac{A_0\omega}{T_{1\mathrm{H}}(\omega)}, \qquad (1)$$

where A_0 is a constant, which is insensitive to temperature or frequency, and is determined by the type of NMR active group.

Recently, some progress has been made in the theoretical studies of the orientational mobility of dendrimers,[41–45] which provides an insight into the factors influencing the position of the maximum.[46,47] In particular, it has been established[46] that the frequency dependence of $[1/T_1]$ for a labeled segment of a dendrimer is determined by three processes with different characteristic times. The first process corresponds to the local reorientation motions of the segment with the relaxation time, τ_{loc}, which does not practically depend on the dendrimer size and on the topological location of the segment. The second process correlates with the rotation of a dendrimer branch that originates from this segment, where the characteristic time, τ_{br}, of this process depends only on the branch size. The last process is the rotation of a dendrimer as a whole with the characteristic time, τ_{rot}, which depends on the dendrimer size. These results were obtained for the following dendrimer models: (i) the viscoelastic model consisting of the Gaussian subchains, and (ii) the freely jointed bead–rod model. The first model was considered in terms of the analytical theory, while the second one was simulated by the Brownian dynamics method. Dendrimers up to the generation number $n = 4$ were studied.

On the basis of these results, the frequency dependences of $[1/T_1]$ for segments of a dendrimer belonging to different dendrimer layers were calculated. For both models, the independence of $\omega_{\max}$ from n and from the location of the segment inside a dendrimer was demonstrated. This independence is explained by the fact that $\omega_{\max}$ is mainly determined by the local reorientation motions of the segment. Therefore, one can expect[39] that the position of the temperature maximum of $[1/T_1]$ at ω = const is also insensitive to n and to the segment location. However, this prediction does not agree with the experimental data.[32,35–37]

It has been assumed[47] that this discrepancy is connected with a restricted flexibility (semiflexibility) of a dendrimer. The effect of the dendrimer semiflexibility has been introduced into the viscoelastic model through the correlations between orientations of segments belonging to different dendrimer layers,[48–50]

$$|\langle \boldsymbol{u}_i \boldsymbol{u}_j \rangle| = q^k, \qquad (2)$$

where $\boldsymbol{u}_i$ and $\boldsymbol{u}_j$ are unit vectors directed along the ith and jth segments separated by kth segments and a parameter of semiflexibility in this model, q, is the average cosine of the angle between neighbouring segments. Indeed, the calculations of the frequency dependence of $[1/T_1]$ for the dendrimer segments have shown that the incorporation of the restricted flexibility into the model leads to the dependence of $\omega_{\max}$ on the dendrimer layer number of the labeled segment.[47] The analysis has demonstrated that the decrease of flexibility leads to a corresponding decrease of the contribution of local processes to the frequency dependence of $[1/T_1]$, as well as to the increase of the contribution of the second process connected to the rotation of a dendrimer branch originating from a labeled segment.

It is necessary to bear in mind, however, that these conclusions have been drawn for the viscoelastic model, where the volume and hydrodynamic interactions are not taken into account. Moreover, the viscoelastic model describes incorrectly the third process, *i.e.* the rotation of a dendrimer as a whole.[46]

In the present work, we study the behavior of $[1/T_1]$ for segments of the poly-L-lysine (PLL) dendrimer on the basis of the full-atomic molecular dynamic (MD) simulations. It is shown that these dendrimers exhibit different positions of the maxima of the $1/T_1$ frequency and temperature dependences for terminal and inner segments. We explain such a difference by the restricted flexibility of the PLL dendrimers.

This paper is structured as follows: in Section II we briefly describe the model and simulation details. Section III is devoted to our results and their discussion. Eventually, Section IV contains the conclusions. Some calculation details are presented in Appendices A and B.

II. Molecular dynamic simulation details

The chemical structure of PLL dendrimers is shown in Fig. 1. There are two segments originating from every branching point, which are characterized by different lengths. The inner longer segments are about 2.5 times larger than the shorter ones. The length ratio of terminal segments is close to 5.

In this paper, the numeration of dendrimer layers, m, in every dendrimer starts from the *periphery* to the core, *i.e.* $m = 0$ corresponds to the terminal layer and $m = n$ corresponds to the core (see Fig. 1).

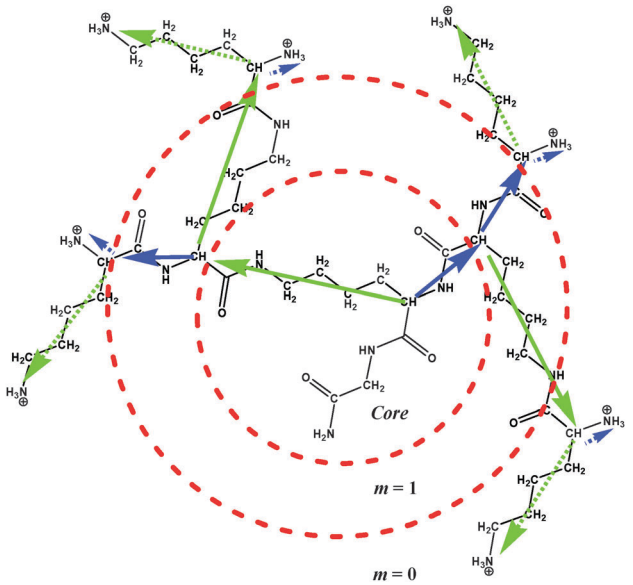

Fig. 1 The chemical structure of the n = 1 generation PLL dendrimer. The solid blue and green arrows are the vectors connecting C atoms of branching points for short and long inner segments, respectively. The dotted arrows are the vectors connecting C atoms of terminal branching points and N atoms of terminal NH_3 groups. m is the dendrimer layer number.

Table 1 Main characteristics of the PLL dendrimers. n is the number of generations, N_{in} is the number of inner segments and N_t is the number of terminal segments

n	M (g mol^{-1})	N_{in}	N_t
2	2028	15	16
3	4095	31	32
4	8229	63	64
5	16 496	127	128

The detailed description of the full-atomic model of the PLL dendrimer used in this work, and the simulation method, including the preparation and equilibration of the system, has been given in our previous work.[51] In brief, the dendrimers of n = 2–5 generations with protonated NH_3^+ terminal groups were studied in the dilute water solution. Some parameters of the dendrimers are collected in Table 1. The cubic simulation box contains a single dendrimer molecule and water molecules together with Cl^- counterions. The number of Cl^- counterions is equal to the number of charged NH_3^+ terminal groups in the dendrimers. For the simulation of water molecules, a TIP3P model[52] was used. The periodical boundary conditions and the Amber99sb-ildn force field were used,[53] and calculations were performed in the *NPT* ensemble. Trajectories at 300 K for n = 2–5 and at Θ = 283, 323, 343 and 363 K for n = 2 and 4 were obtained. Here and thereafter, Θ is the absolute temperature. The Gromacs-4.5.5 package was used for our simulations.[54] First, 50 ns of each MD simulation were applied for the equilibration of the system, and final 150 ns for calculations of the system characteristics. The sizes of the n = 2–4 dendrimers, obtained from our simulation, are in good agreement with the experimental data.[55] Our results for the n = 3 dendrimer agree also with those obtained in ref. 56.

In the PLL dendrimer, the lengths of segments in the same dendrimer layer are different in contrast to the theoretical model,[47] where all segments have the same length. We believe that this difference is not important for the effect of the semiflexibility on the segmental orientation mobility. This assumption is supported by similar characteristics of the orientation mobility of the long and short segments belonging to the same layer in the PPL dendrimer.[40]

Semiflexibility parameter

In order to compare our simulation results with the predictions of the semiflexible viscoelastic theory,[47] which were obtained for the semiflexibility parameter q = 0.45 in eqn (2), it is necessary to estimate the value of q for the PLL dendrimer with the results of our MD simulation.

We have calculated the average angle, θ, between the neighboring segments belonging to two successive dendrimer layers (Table 2). The value of θ averaged over different n values is found to be equal to 119°, which corresponds to q = 0.48 in eqn (2). This value is close to q = 0.45 (θ = 117°) used in ref. 47. Therefore, we can compare directly our simulation results with the theoretical calculations performed in ref. 47.

Theory of the spin–lattice NMR relaxation

The spin–lattice ^{1}H NMR relaxation for NMR active groups in terms of the dipole–dipole interaction of relaxation is given by the following equation:[39]

$$\frac{1}{T_{1H}}(\omega_H, \Theta) = A_0(J(\omega_H, \Theta) + 4J(2\omega_H, \Theta)) \quad (3)$$

where ω_H is the angular frequency of the used spectrometer for ^{1}H atoms, the spectral densities $J(\omega,\Theta)$ and $J(2\omega,\Theta)$ are real parts of the Fourier transform of the second-order orientation ACF, $P_2(t)$, for the vector between ^{1}H atoms in the CH_2 groups, $\boldsymbol{r}_{HH}$ (see Fig. 2):[39]

$$J(\omega) = 2\int_0^\infty P_2(t)\cos(\omega t)\mathrm{d}t \quad \text{and} \quad J(2\omega) = 2\int_0^\infty P_2(t)\cos(2\omega t)\mathrm{d}t. \quad (4)$$

Here,

$$P_2(t) = \frac{3}{2}\left(\left\langle \boldsymbol{u}(t)\boldsymbol{u}(0)^2\right\rangle - \frac{1}{3}\right), \quad (5)$$

where $\boldsymbol{u}(t) = \boldsymbol{r}_{HH}/|\boldsymbol{r}_{HH}|$ is a unit vector. The function $J(\omega)$ was calculated from P_2 ACF numerically using eqn (4). The details of the calculation are given in Appendix A.

Table 2 The average angle (θ) between the neighboring segments belonging to two successive dendrimer layers in PLL dendrimers with n = 2–5

	θ (degrees)			
Θ (K)	n = 2	n = 3	n = 4	n = 5
283	118 ± 4	—	122 ± 3	—
300	118 ± 4	120 ± 2	120 ± 2	120 ± 2
323	119 ± 2	—	121 ± 1	—
343	118 ± 4	—	120 ± 1	—
363	118 ± 5	—	120 ± 1	—

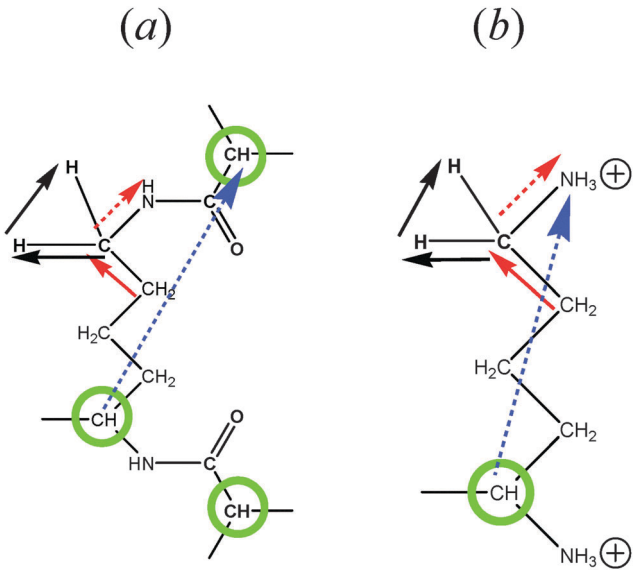

Fig. 2 Chemical structure of an internal segment (a) and a terminal segment (b). The green circles mark branching points. The black arrows correspond to the direction of $\boldsymbol{r}_{HH}$ and $\boldsymbol{r}_{CH}$ unit vectors of CH_2 groups, which are observed in the NMR relaxation. The red arrows are $\boldsymbol{r}_{CC}$ and $\boldsymbol{r}_{CN}$ vectors of CC and CN bonds, which are connected in the CH_2 group, and the dotted blue arrows mark the long segment vector, $\boldsymbol{r}_s$. The orthogonal vector is determined by the expression $\boldsymbol{r}_{tr} = [\boldsymbol{r}_{CC} \otimes \boldsymbol{r}_{CN}]$.

If $P_2(t)$ is represented by the sum of exponents,

$$P_2(t) = \sum_l C_l^* \exp(-t/\tau_l^*), \quad (6)$$

where C_l^* and τ_l^* are the weights of the relaxation times; the spectral density can be expressed as

$$J(\omega) = 2\sum_l \frac{C_l\tau_l^*}{1 + (\omega\tau_l^*)^2} \quad (7)$$

III. Results and discussion

Comparison with the analytical theory

The minimum length scale of the viscoelastic model corresponds to the length of a single segment. Therefore, to compare with the analytical theory it is necessary to study the reorientation of the unit vectors directed along the segments (Fig. 2), *i.e.* $\boldsymbol{u}(t) = \boldsymbol{r}_s(t)/|\boldsymbol{r}_s(t)|$ in the PLL dendrimers. We consider the reduced relaxation rate, $[1/T_{1H}]$, given by eqn (1) as well as in ref. 46 and 47. The calculation methods of $[1/T_{1H}]$ at different frequencies ω for the segments belonging to different dendrimer layers, using the simulation data, are described in Appendix A.

Fig. 3 shows the frequency dependences of $[1/T_{1H}]$ for the segments belonging to different dendrimer layers m of the PLL

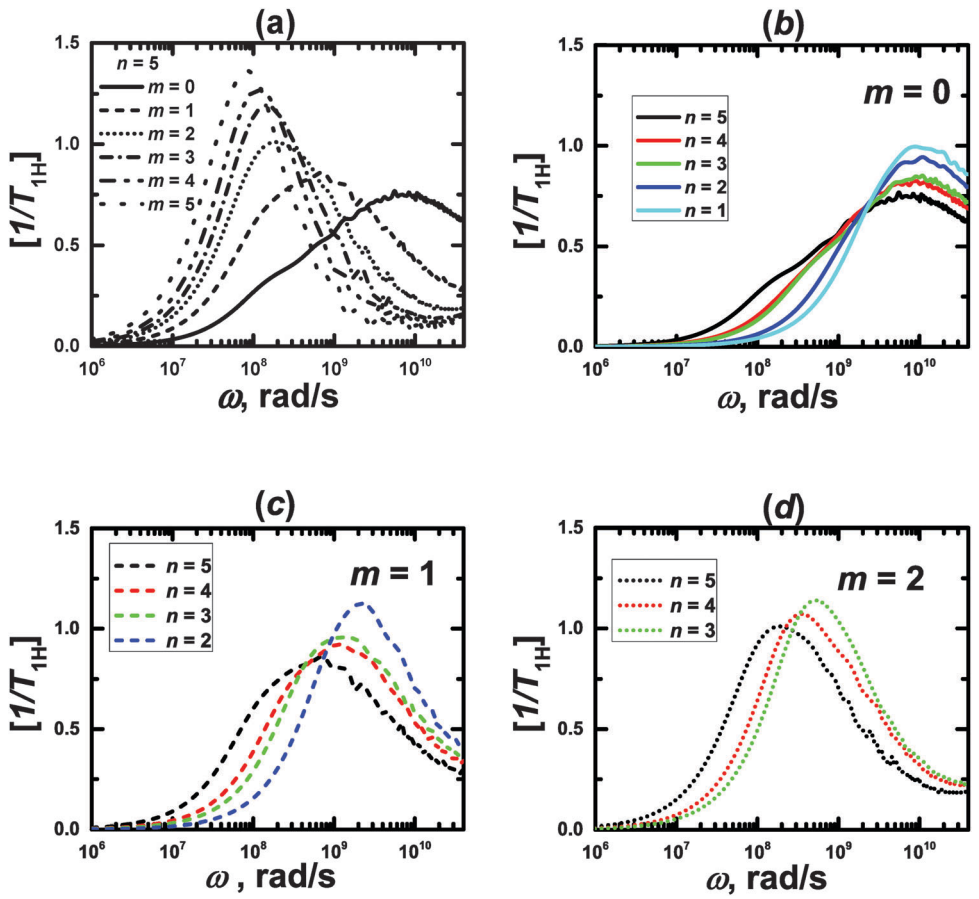

Fig. 3 Frequency dependences of $[1/T_{1H}]$ for the segments of lysine dendrimers. MD simulation results.

dendrimers with different n. It can be seen that the position of $[1/T_{1H}]$ maximum ω_{max} depends on the layer number, m (Fig. 3a). When m increases, ω_{max} shifts towards lower frequencies.

This result agrees qualitatively with the predictions of the analytical theory for the semiflexible viscoelastic model of the dendrimer.[47] Here we recall that the flexible viscoelastic model predicts the independence of ω_{max} from m.

As in the viscoelastic model, the simulated ω_{max} for the terminal segments (m = 0) is practically independent from n (Fig. 3b). Hence, we can use the value of $\omega_{max}(m = 0) = \omega_0$ as the reference point in order to compare the results of the analytical theory with the simulations. Fig. 4 shows the values of ω_{max}/ω_0 for different m and n obtained from the theory[47] for the semiflexible dendrimer and our simulation results. It can be seen that the overall trend is the same: ω_{max}/ω_0 decreases with increasing m. However, there are some differences between the theory and the simulation. First, the simulation demonstrates that ω_{max} for given m depends on the overall generation number n of a dendrimer, in contrast to the theory predictions about the insensitivity of $\omega_{max}(m$ = const) to n. Second, the theory predicts a more rapid decrease of ω_{max} with m for $m \geq 2$ than that obtained with the simulations.

The following connects these differences with the simplifications used in the viscoelastic dendrimer model. First, the model does not take into account the excluded volume and hydrodynamic interactions (the phantom and free-draining model). Therefore, the segments in this model do not "feel" the local concentration of surrounding segments in the dendrimer. However, this concentration can depend on n for the segments with the same m, and affect their orientation mobility. Our previous simulation shows[51] that the average density of PLL dendrimers grows with n. Therefore, the local concentration of dendrimer monomers in internal layers is expected to increase as well, which could lead to an increase of τ_{br} due to additional friction between the branch and other segments of the dendrimer and a decrease of ω_{max}.

The second defect of the viscoelastic model is its inability to describe correctly the contribution of the dendrimer rotation as a whole to the segment relaxation. The simulations of the coarse-grained dendrimer models[46] in solution show that this

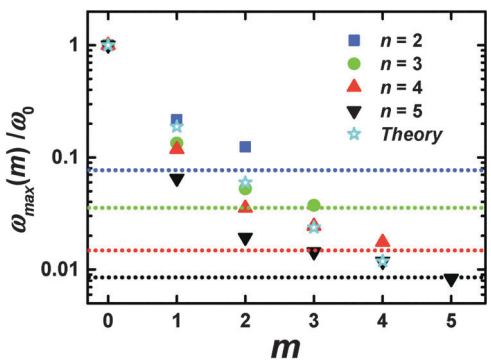

Fig. 4 The position of the $[1/T_{1H}]$ maxima for different m and n. Dotted horizontal lines mark ω_{rot} and correspond to n with the same color; $\omega_0 = \omega_{max}(m = 0)$. MD simulation and analytical theory[47] results.

Table 3 Characteristic times of the rotation PLL dendrimers as a whole, τ_{rot}, at 300 K

n	τ_{rot} (ns)
2	0.8 ± 0.04
3	1.7 ± 0.1
4	4.2 ± 0.2
5	7.2 ± 0.2

contribution can be quite significant. The values of τ_{rot} for the PLL dendrimers with n = 2–5 at 300 K, calculated in Appendix B, are collected in Table 3.

If the orientational relaxation of a segment is determined only by the dendrimer rotation as a whole, ω_{max} will be equal to ω_{rot} related to τ_{rot} with the expression

$$\omega_{rot} \approx \frac{0.616}{\tau_{rot}} \quad (8)$$

(see *e.g.* page 203 of ref. 57). The values of ω_{rot} for different n are shown by horizontal dotted lines in Fig. 4. It can be seen that for segments with $m = n$ the values of ω_{max} are equal to $\omega_{rot}(n)$, which means that the reorientation of the segments lying close to the core is determined by the rotation as a whole. For lower m, the relation $\omega_{max}(m,n) > \omega_{rot}(n)$ means that the internal modes start to contribute to the segment reorientation. However, the observed splitting of ω_{max} for different n and the same m shows that the contribution of the rotation as a whole affects remarkably the value of ω_{max}.

Finally, we can conclude that the shift of ω_{max} towards lower frequencies with the increase of m observed in the simulations can be described by the effect of the semiflexibility, predicted by the analytical viscoelastic model.[47] For the segments lying close to the dendrimer core, this shift is decreased due to the increased contribution of the dendrimer rotation as a whole.

Spin–lattice NMR relaxation of CH_2 groups

MD simulations of the full-atomic model allow the study not only of the reorientation of the segments, but also of the mobility of NMR active groups. We focus mainly on the mobility of $\boldsymbol{r}_{HH}$ vectors in CH_2 groups (which are connected to N atoms) for the PLL dendrimer in water. The temperature dependences of $1/T_{1H}$ for these $\boldsymbol{r}_{HH}$ vectors were measured in our NMR experiments.[40]

The method of the spin–lattice NMR relaxation allows one to measure proton relaxation time, T_{1H}, separately for groups with different chemical shifts, *i.e.* with different peak positions of the ^{1}H NMR spectrum. The value of the shift for the same group depends on the chemical structure of its environment. In principle, the NMR active groups located in different dendrimer layers may correspond to different peaks. In particular, this situation is realized for poly(aryl ether) dendrimers.[37] It allows the mobility in every dendrimer layer to be studied separately. In the case of the PLL dendrimer, there is a remarkable difference of the chemical shifts between terminal and inner CH_2–N groups, but it is difficult to distinguish the difference between inner layers (see ESI).

Therefore, to compare the simulation data with the experimental spin–lattice relaxation rate for the inner CH_2–N groups, $[1/T_{1H}^{inn}]$, we have to use in eqn (5) the function $P_2^{inn}(t)$ averaged over all inner groups:

$$P_2^{inn}(t) = \frac{\sum_{m=1}^{n} N_m P_2(t,m)}{\sum_{m=1}^{n} N_m}, \quad (9)$$

where $N_m = 2^{n-m+1}$ is the number of long segments in the mth dendrimer layer.

We have calculated frequency dependences of $[1/T_{1H}^{inn}]$ and $[1/T_{1H}^{ter}]$ at different temperatures, Θ, for CH_2 groups in PLL dendrimers by using eqn (3)–(5) and (9) with a unit vector $\boldsymbol{u}(t) = \boldsymbol{r}_{HH}(t)/|\boldsymbol{r}_{HH}(t)|$. Here, $[1/T_{1H}^{ter}]$ depends on $\boldsymbol{r}_{HH}$ of the terminal long groups (see Fig. 2b). The details of the calculations are described in Appendix A.

For both studied dendrimers (n = 2 and 4) at all temperatures, the positions of ω_{max} of the maximum of $[1/T_{1H}]$ for the $\boldsymbol{r}_{HH}$ vectors of the CH_2 terminal groups are shifted to higher frequencies with respect to those of the CH_2 inner groups (Fig. 5). Therefore, the shift of ω_{max} with increasing dendrimer layer number, observed above for the segments, takes place also for the NMR active groups. We believe that in both cases this shift is the manifestation of the dendrimer semiflexibility effect.

For the same segments, the values of ω_{max} for $\boldsymbol{r}_{HH}$ exceed those for $\boldsymbol{r}_s$ (Fig. 6). However, this difference is not connected with the different sizes of the CH_2 groups and segments. Therefore, we have calculated the frequency dependences of the $[1/T_{1H}]$ functions for $\boldsymbol{r}_{CC}$, which has approximately the same length as $\boldsymbol{r}_{HH}$ (Fig. 6). It can be seen that these dependences practically coincide with those for $\boldsymbol{r}_s$. At the same time, the frequency dependences of $[1/T_{1H}]$ for $\boldsymbol{r}_{HH}$ are shifted towards higher values. We believe that this difference can be explained by the fact that the reorientations of the $\boldsymbol{r}_{HH}$ vectors correspond to transversal modes, in contrast to those of $\boldsymbol{r}_s$, which are determined by longitudinal modes. As has been shown in several studies (see *e.g.* ref. 58), the transversal modes are considerably faster than the longitudinal ones.

Comparison with NMR experimental data

Here we compare the results of the MD simulations with the experimental results obtained in our work.[40] The circle frequency of the spectrometer, which is used in ref. 40 was

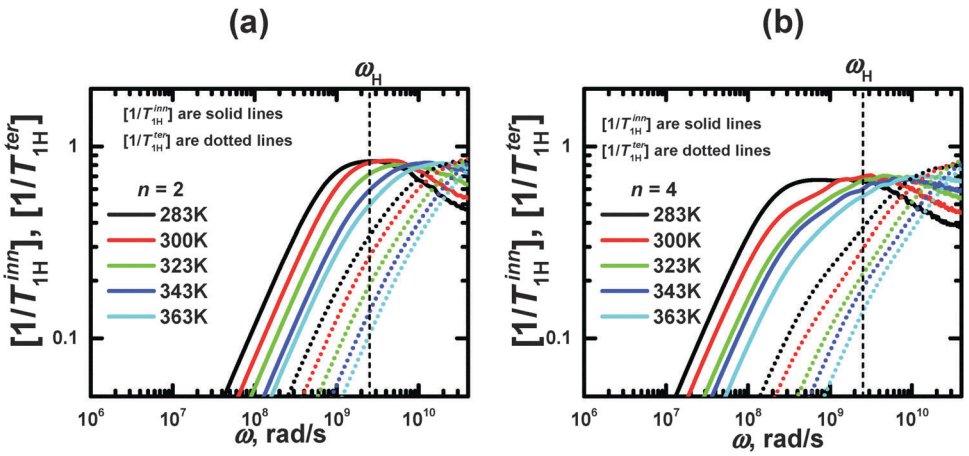

Fig. 5 Frequency dependences of $[1/T_{1H}]$ for $_2$ groups of inner and terminal segments of lysine dendrimers with n = 2 and 4. The vertical dotted line indicates the frequency ($\omega_H/2\pi$ = 400 MHz) corresponding to the spectrometer used in ref. 40.

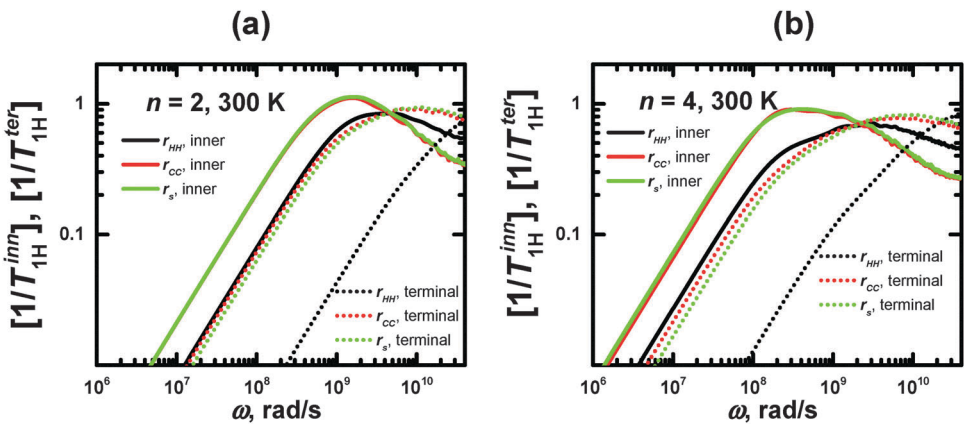

Fig. 6 Frequency dependences of $1/T_{1H}$ for $\boldsymbol{r}_{HH}$, $\boldsymbol{r}_{CC}$, and $\boldsymbol{r}_s$, calculated for inner and terminal segments of lysine dendrimers with n = 2 and 4 at 300 K.

$\omega_H/2\pi$ = 400 MHz. In Fig. 5 this frequency is marked by a vertical dotted line. The crossing points of the simulated frequency dependences of $[1/T_{1H}]$ at different temperatures with this line give the values of $[1/T_{1H}]$ corresponding to those obtained experimentally. For the direct comparison of our results with experimental data, it is necessary to know the value of A_0 in eqn (3). In the case of the CH_2 groups,[39,57] this constant is given by the expression

$$A_0 = \frac{3}{10}\left(\gamma_H^4 \hbar^2 / r_{HH}^6\right), \qquad (10)$$

where γ is a gyromagnetic ratio of ^1H and r_{HH} is the effective distance between protons. If we use the value of $A_0^{theor} = 0.56 \times 10^{10}$ s^{-2}, calculated from eqn (10), we obtain a remarkable difference between the results of the MD simulation and the experimental data. This is a typical situation for dendrimers (see *e.g.* experimental results in ref. 32, 35 and 36). Due to this fact, the value of A_0 is considered as a fitting parameter and is determined by the coincidence of the experimental and the simulated $1/T_{1H}$ data at 300 K. The values of $A_0^{inn} = 0.35 \times 10^{10}$ s^{-2} and $A_0^{ter} = 0.51 \times 10^{10}$ s^{-2} were obtained for the CH_2 groups, belonging to the inner segments and the terminal CH_2 groups, respectively. The answer to the question about the reasons for the difference between these values and A_0^{theor} can be obtained only by quantum chemistry methods. We can suggest one possible variant: experimental values of $|r_{HH}|^{-6}$ differ from theoretical ones, calculated using standard values of the C–H chemical bond and the valence angle for the CH_2 group. Fig. 7 shows the temperature dependences of $1/T_{1H}$, obtained with the simulation data using the corresponding values of A_0 and the experimental temperature dependences of $1/T_{1H}$. It can be seen that the simulation results reproduce the experimental data. Unfortunately, because the accessible temperature interval is limited by the boiling and freezing points of the solvent, this does not allow the observation of all the maxima of $1/T_{1H}$. For the inner groups, the function $1/T_{1H}(\Theta^{-1})$ has a maximum within the measured temperature interval. For the terminal groups, this maximum of $1/T_{1H}$ grows almost exponentially with increasing Θ^{-1}.

The temperature dependences, $1/T_{1H}(\Theta^{-1})$, for the inner and terminal groups of the PLL dendrimers were obtained at the fixed frequency ($\omega_H/2\pi$ = 400 MHz). However, the shape and the relative positions of the $1/T_{1H}(\Theta^{-1})$ curves depend not only on the location of the active groups inside a dendrimer, but on the spectrometer frequency $\omega_H/2\pi$, as well. In particular,

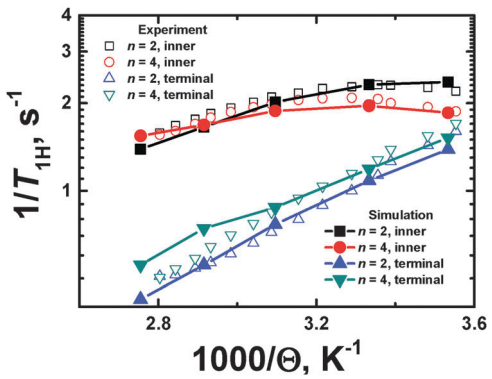

Fig. 7 Plots of $1/T_{1H}$ *vs.* inverse temperature ($1000/\Theta$) for terminal and inner CH_2 groups. The NMR experimental data[40] and the MD simulation results are shown.

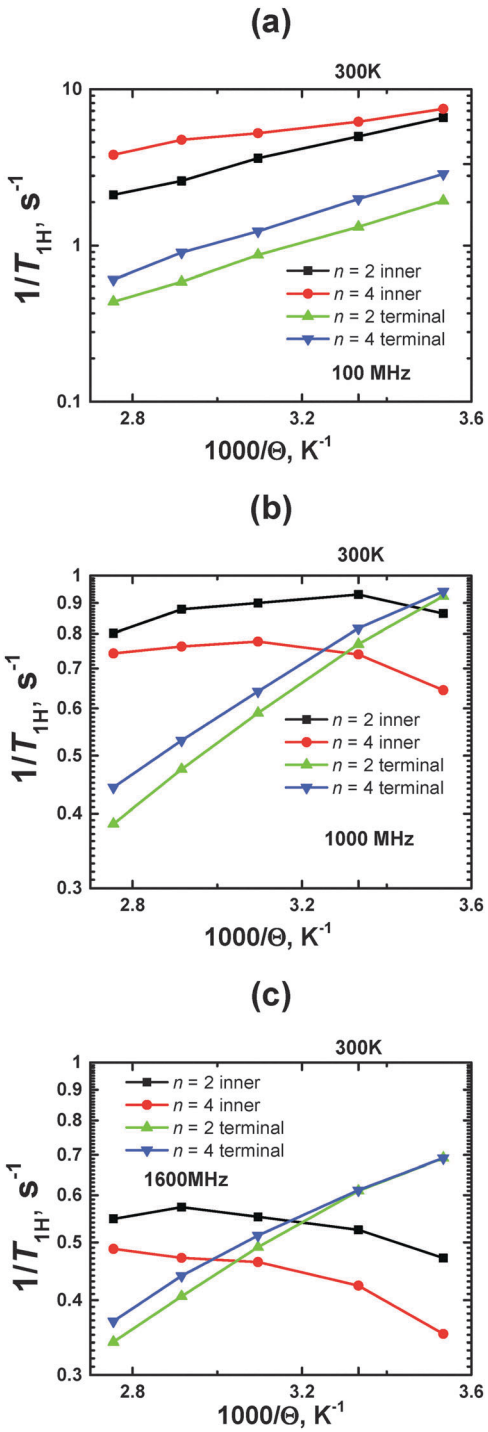

Fig. 8 Plots of $1/T_{1H}$ *vs.* inverse temperature ($1000/\Theta$) for terminal and inner CH_2 groups at different $\omega_H/2\pi$ = 100, 1000 and 1600 MHz. MD simulation results.

the consideration of the temperature dependence at different frequencies has been performed in ref. 37.

Using the calibration value of A_0, we obtained temperature dependences of $1/T_{1H}$ at $\omega_H/2\pi$ = 100, 1000, and 1600 MHz (Fig. 8).

At a smaller frequency $\omega_H/2\pi$ = 100 MHz, the curves for the inner groups are located higher along the vertical axis, than those for terminal groups, within the whole temperature interval. At higher frequencies ($\omega_H/2\pi \geq 400$ MHz), these curves cross each other, where the crossing points are shifted to higher temperatures with increasing frequency.

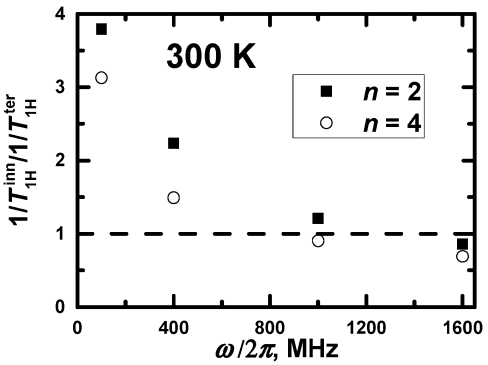

Fig. 9 The ratio of $(1/T_{1H}^{ter})/(1/T_{1H}^{inn})$ at Θ = 300 K *vs.* different frequencies.

As was mentioned in the Introduction, the traditional approach to characterize the mobility of different parts of dendrimers by NMR relaxation focuses on the comparison of the $1/T_{1H}$ values at the same (room) temperature (see *e.g.* ref. 13 and 27–29). It is assumed that the lower value of $1/T_{1H}$ corresponds to the higher mobility. This assumption is completely correct if the measured $1/T_{1H}$ values are located on the left side of the $1/T_{1H}(\Theta^{-1})$ maximum. This case corresponds to the frequency $\omega_H/2\pi$ = 100 MHz, when the curves of the inner groups or terminal groups are shifted to a larger value of $1/T_{1H}$ for n = 4 with respect to those for n = 2; $1/T_{1H}$ points of inner groups have a larger value than ones of terminal groups for the same n. For higher frequencies ($\omega_H/2\pi \geq 1600$ MHz), there is an opposite situation: the values of $1/T_{1H}$ at Θ = 300 K of the terminal groups are found to be larger than those of the inner ones.

In principle, a qualitative comparison of the mobility of the inner and terminal groups in the same PLL dendrimer by $1/T_{1H}$ is possible for frequencies up to 1000 MHz. Fig. 9 shows the ratio of $(1/T_{1H}^{ter})/(1/T_{1H}^{inn})$ for different frequencies, calculated at Θ = 300 K. It can be seen that this ratio exceeds unity at low frequencies and is less than unity at higher

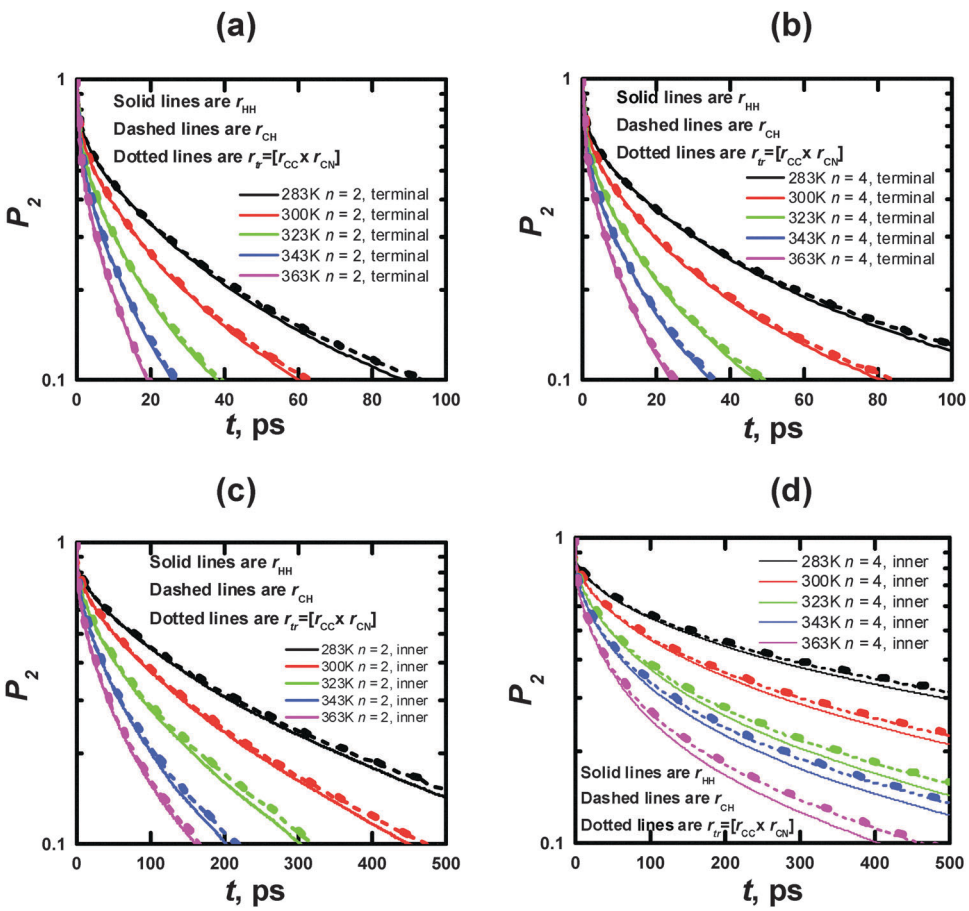

Fig. 10 Time dependences of P_2 obtained from the MD simulations for $\boldsymbol{r}_{HH}$ (solid lines), $\boldsymbol{r}_{CH}$ (dashed lines), and $\boldsymbol{r}_{tr}$ (dotted lines) vectors in terminal (a, c) and inner (b, d) CH_2 groups (cf. Fig. 2a and b) at different temperatures.

1000 MHz frequencies. This result is obtained from the large difference in the orientational mobility of inner and terminal groups due to low flexibility of segments in the PLL dendrimers. However, this frequency will be lower than 400 MHz if there is a possibility to consider the $1/T_{1H}$ values of groups from the different inner layers. This result is expected due to $1/T_{1H}$ data for segments (see Fig. 3a). A quantitative comparison of the mobility of inner and terminal groups of the same dendrimer using $1/T_H$ is possible also at frequencies lower than 400 MHz.

Thus, our results for PLL dendrimers confirm the conclusions of ref. 37 that the traditional approach can lead to incorrect conclusions and, therefore, the features of the temperature dependence of $1/T_1$ are important for the interpretation of the $1/T_1$ data for dendrimers.

Experimentally, the decrease of the angular frequency ω_H leads to a deterioration in the resolution of a spectrometer. This difficulty can be avoided by the use of ^{13}C atoms to measure the NMR relaxation, because $\omega_H/\omega_C \approx 4$ for the same spectrometer.[30] The $1/T_{1C}$ function for carbon atoms is determined by the following equation:[39,57]

$$1/T_{1C}(\omega_C) = A_0(C)[6J(4.97\omega_C) + J(2.97\omega_C) + 3J(\omega_C)], \quad (11)$$

and by eqn (4) and (5), where $\boldsymbol{u}(t) = \boldsymbol{r}_{CH}$ (see Fig. 2). In Fig. 10, the time dependences of P_2 ACF for the $\boldsymbol{r}_{HH}$ and $\boldsymbol{r}_{CH}$ vectors are displayed, which determine the frequency dependence of the $1/T_{1H}$ and $1/T_{1C}$ functions. It can be seen that these functions practically coincide with each other and correspond to P_2 ACF for the $\boldsymbol{r}_{tr}$ vector. Therefore, NMR relaxations for ^1H or ^{13}C atoms are determined by the same relaxation processes, and all conclusions for PLL dendrimers concerning $1/T_{1H}$ are valid for $1/T_{1C}$.

IV. Conclusions

The temperature and frequency dependences of the spin–lattice NMR relaxation rates $(1/T_1)$ for the segments and the NMR active CH_2 groups in poly-L-lysine dendrimers in water have been calculated on the basis of full-atomic molecular dynamics simulations. The comparison of the simulation results with the theoretical predictions for the viscoelastic model, developed recently in ref. 47, has been performed. It shows that the observed dependence of the position of the $[1/T_1]$ maximum on the location of the segments inside the dendrimer can be explained by the effect of the restricted flexibility of a dendrimer. The same effect can be responsible for the difference in the orientational mobility of the terminal and inner NMR active CH_2 groups in PLL dendrimers. This difference leads to the different temperature dependences of $1/T_{1H}$ for the terminal and inner groups, observed experimentally by us in ref. 40. Our simulations reproduce the experimental data for $n = 2$ and $n = 4$ PLL dendrimers.

Since the differences in the temperature dependence of $1/T_{1H}$ for the inner and terminal groups have been observed also for other dendrimers,[32,35] we can suppose that the restricted flexibility (semiflexibility) manifests itself in these

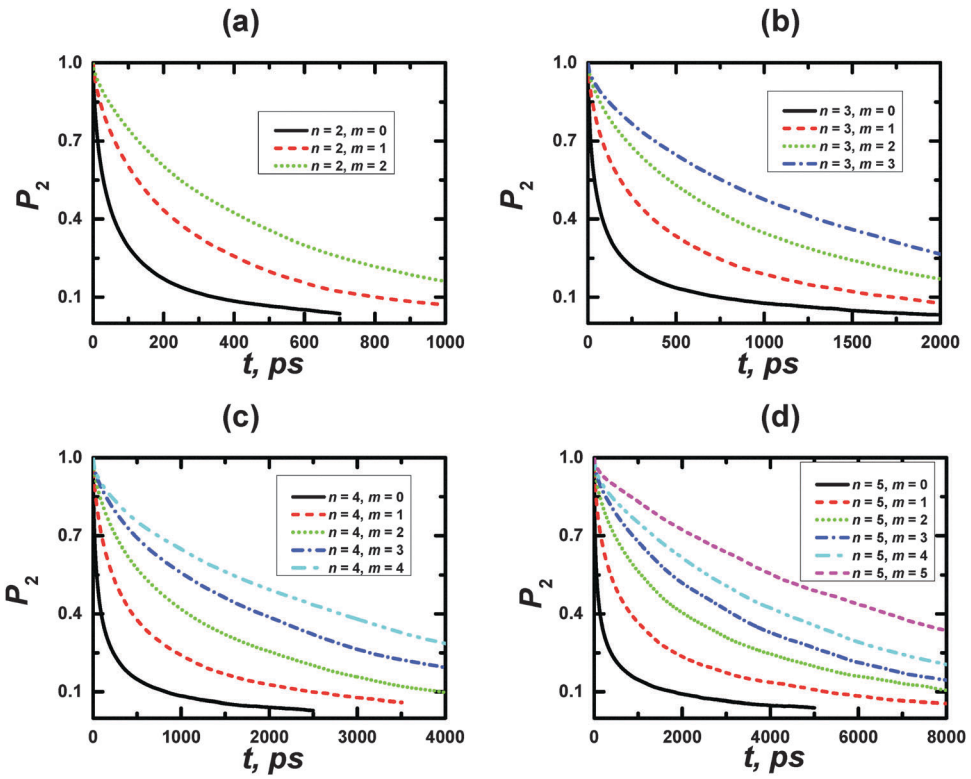

Fig. 11 Time dependencies of P_2 ACF for segments of PLL dendrimers with $n = 2$–5 at $\Theta = 300$ K.

cases, as well. The similar effect can also be responsible for the different temperature dependences of $1/T_{1H}$ for NMR active groups in different layers of poly(aryl ether) dendrimers.[37]

In our work the applicability of the traditional interpretation of the NMR experimental data, when the smaller values of $1/T_1$ correspond to the higher orientation mobility, is also discussed. We have confirmed the conclusion of ref. 37 to consider the temperature dependence of $1/T_1$ for the correct interpretation of the $1/T_1$ data for dendrimers. We have calculated the temperature dependences of $1/T_{1H}$ for inner and terminal groups in PLL dendrimers at different frequencies. It is shown that the traditional procedure is applicable for the comparison of the mobility of inner and terminal groups of different PLL dendrimers at the room temperature only at low frequencies ($\sim$100 MHz). At high frequencies ($\geq$1600 MHz), the opposite situation is observed: the smaller values of $1/T_{1H}$ correspond to the lower mobility.

Concerning the mobility of the inner groups of the different PLL dendrimers, the procedure above is correct only at frequencies below $\sim$400 MHz. In the same case of the terminal groups, the traditional approach can be applied within the experimentally accessible frequency interval.

A qualitative comparison of the mobility of the inner and terminal groups in the same PLL dendrimer by $1/T_{1H}$ is possible for frequencies up to 1000 MHz. This result is obtained from the large difference in the orientational mobility of inner and terminal groups due to the low flexibility of segments in the PLL dendrimers. However, this frequency will be lower than 400 MHz if there is a possibility to consider the $1/T_{1H}$ values of groups from the different inner layers ($m > 0$). Also, a quantitative comparison of the mobility of inner and terminal groups of the same dendrimer using $1/T_H$ is possible also at frequencies lower than 400 MHz.

Additionally, we have shown that the ^{1}H or ^{13}C NMR relaxations for PLL dendrimers are determined by the same relaxation processes. Therefore, the main conclusions concerning

Table 4 Characteristic times of P_2 ACF for the $\boldsymbol{r}_s$ vectors of the PLL dendrimer segments with n = 2–5 at 300 K

	τ_{tail} (ps)					
n	m = 0	m = 1	m = 2	m = 3	m = 4	m = 5
2	373	505	1190	—	—	—
3	1092	1281	1407	1465	—	—
4	1797	2004	2246	2702	3092	—
5	3267	4528	4809	4939	5564	7610

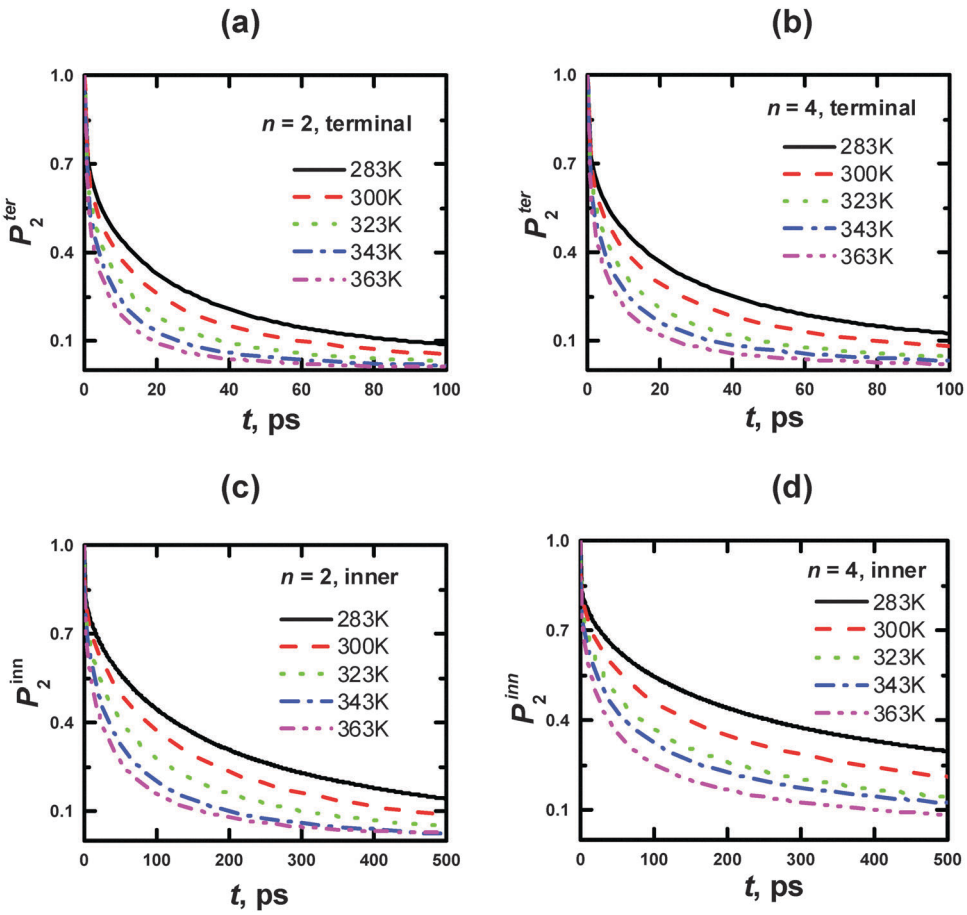

Fig. 12 Time dependences of P_2 ACF for the $\boldsymbol{r}_{HH}$ vectors of CH_2 groups of the PLL dendrimer terminal (a, b) and inner (c, d) segments with n = 2 (a, c) and 4 (b, d) at different temperatures.

$1/T_{1H}$ are applicable also to $1/T_{1C}$. Thus, the use of these two methods provides mutually complementary information about molecular mobility in PLL dendrimers.

Appendix A

Calculations of the frequency dependences of $1/T_{1H}$ functions.

To obtain $1/T_{1H}$ functions from P_2 ACF, we use numerical calculations on the basis of eqn (4) for spectral density, which determines $1/T_{1H}$ in eqn (3). To improve the numerical calculation results, we approximate the tail of each P_2 ACF by one-exponential fitting and construct full P_2^{full} using eqn (A.1):

$$P_2^{full}(t) = \begin{cases} P_2(t); & t \le t_{cut} \\ P_2(t = t_{cut})\exp(-t/\tau_{tail}); & t > t_{cut} \end{cases}, \quad (A.1)$$

where t_{cut} is the cutting time for each P_2 ACF, τ_{tail} is the characteristic time, which is calculated from the finite slope of the P_2 ACF. For all curves, we use t_{cut} given by the condition of $P_2(t_{cut}) \le 0.01$.

This method is applied to the calculation of $[1/T_{1H}]$ functions. Initial data are presented for different vectors of PLL dendrimers at several temperatures, including Fig. 11 and Table 4 for $\boldsymbol{r}_s$ vectors of the segments at 300 K, Fig. 12 and Table 5 for $\boldsymbol{r}_{HH}$ vectors of the inner and terminal segments in the dendrimers with n = 2 and 4 at 283, 300, 323, 343, 363 K, and Fig. 13 and Table 6 for $\boldsymbol{r}_{CC}$ vectors of the inner and terminal segments in the dendrimers with n = 2 and 4 at 300 K.

Table 5 Characteristic times of P_2 ACF for the $\boldsymbol{r}_{HH}$ vectors of the PLL dendrimer inner and terminal groups with n = 2 and 4 at different temperatures

	τ_{tail} (ps)			
	n = 2		n = 4	
Θ (K)	Terminal	Inner	Terminal	Inner
283	295	481	714	2049
300	169	336	667	2017
323	136	292	269	1680
343	76	265	156	1310
363	56	254	92	1188

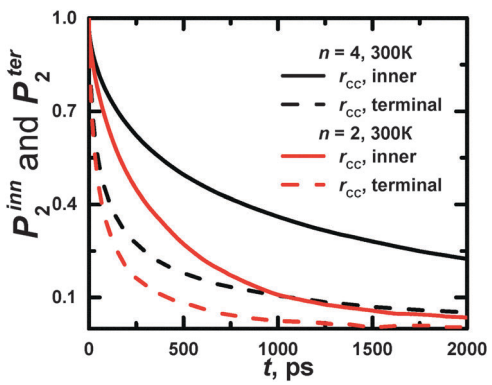

Fig. 13 Time dependences of P_2 ACF for the $\boldsymbol{r}_{CC}$ vectors in inner and terminal segments of PLL dendrimers with n = 2 and 4 at 300 K.

Table 6 Characteristic times of P_2 ACF for the $\boldsymbol{r}_{CC}$ vectors of the PLL dendrimer inner and terminal groups with n = 2 and 4 at 300 K

	τ_{tail} (ps)			
	n = 2		n = 4	
Θ (K)	Terminal	Inner	Terminal	Inner
300	415	787	1806	2558

Appendix B

Characteristic times of rotation of PLL dendrimers as a whole at 300 K.

The characteristic time of rotation of the dendrimer as a whole can be obtained from the P_1^{rot} autocorrelation function (ACF):[41,42]

$$P_1^{rot} = \langle \boldsymbol{r}_d(0)\boldsymbol{r}_d(t)\rangle, \quad (B.1)$$

where $\boldsymbol{r}_d(t)$ is a unit vector along the direction from the core to terminal groups (*i.e.* to NH_3 charged group). The averaging in eqn (B.1) is performed for all the terminal NH_3 groups. The calculated P_1^{rot} ACF data for n = 2–5 generation PLL dendrimers at 300 K are shown in Fig. 14.

The slope of the $\ln(P_1^{rot})$ function corresponds to the reciprocal characteristic time of rotation of a dendrimer as a whole. The dotted lines are the approximation of the slope of $\ln(P_1^{rot})$ in Fig. 14. The results of the calculations are collected in Table 7.

Additionally, we have to point out that the P_2 ACF appears in NMR relaxation and (eqn (B.1)) decays faster than the P_1 ACF. To establish the appearance of $\tau_{rot}^{P_1}$ in P_2 ACF, we calculate P_2^{rot} ACF for the same $\boldsymbol{r}_d$ vector as in eqn (B.1),

$$P_2^{rot}(t) = \frac{3}{2}\left(\left\langle \boldsymbol{r}_d(t)\boldsymbol{r}_d(0)^2\right\rangle - \frac{1}{3}\right). \quad (B.2)$$

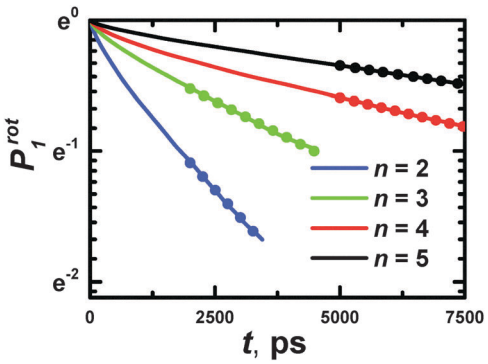

Fig. 14 The time dependencies of P_1^{rot} ACF for PLL dendrimers with n = 2–5 at 300 K. Dotted lines are the approximation of the $\ln(P_1^{rot})$ slope.

Table 7 Characteristic times of the rotation of PLL dendrimers as a whole, $\tau_{rot}^{P_1}$, at 300 K

n	$\tau_{rot}^{P_1}$ (ns)
2	2.4 ± 0.1
3	5.2 ± 0.3
4	12.5 ± 0.5
5	21.6 ± 0.5

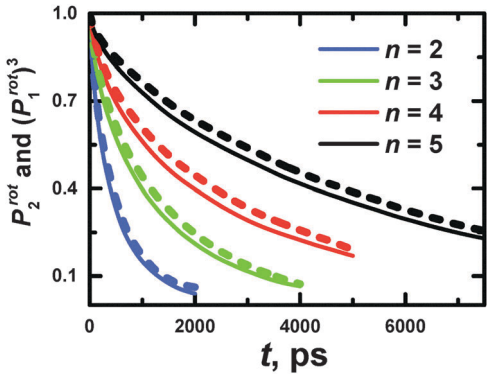

Fig. 15 The time dependencies of P_2^{rot} and $(P_1^{rot})^3$ for PLL dendrimers with n = 2–5 at 300 K.

In Fig. 15, we check up the relationship[42]

$$P_2^{rot}(t) = (P_1^{rot}(t))^3 \quad \text{(B.3)}$$

The utilization of eqn (B.3) seems to be valid for PLL dendrimers, as well. Hence, we can conclude that the rotation time which appears in P_2 ACF, τ_{rot}, is expressed as

$$\tau_{rot} = \tau_{rot}^{P_1}/3. \quad \text{(B.4)}$$

The values of τ_{rot} are presented in Table 3.

Acknowledgements

Many thanks to Dr Konstantin G. Lisunov for helpful discussions. This work is partially supported by the Russian Foundation for Basic Research (grants No. 13-03-00524, 13-03-00728, and 14-03-00926) and the Government of the Russian Federation grant 074-U01. The simulations have been performed using the Lomonosov supercomputers at the Moscow State University and the resources of the computer center of the Saint Petersburg State University.

References

1 E. Buhleier, W. Wehner and F. Vogtle, *Synthesis*, 1978, 155–158.
2 R. G. Denkewalter, J. Kolc and W. J. Lukasavage, *USA Pat.*, 4 289872, 1981.
3 G. R. Newkome, Z.-Q. Yao, G. R. Baker and V. K. Gupta, *J. Org. Chem.*, 1985, **50**, 2003–2004.
4 D. A. Tomalia, H. Baker, J. Dewald, M. Hall, G. Kallos, S. Martin, J. Roeck, J. Ryder and P. Smith, *Polym. J.*, 1985, **17**, 117–132.
5 C. J. Hawker and J. M. J. Fréchet, *J. Chem. Soc., Chem. Commun.*, 1990, 1010–1013.
6 B. K. Nanjwade, H. M. Bechra, G. K. Derkar, F. V. Manvi and V. K. Nanjwade, *Eur. J. Pharm. Sci.*, 2009, **38**, 185–196.
7 E. R. Gillies and J. M. J. Fréchet, *Drug Discovery Today*, 2005, **10**, 35–43.
8 Y. Cheng, *Dendrimer-Based Drug Delivery Systems: From Theory to Practice*, John Wiley and Sons, New York, 2012.
9 J. Wu, W. Huang and Z. He, *Sci. World J.*, 2013, 630654.
10 B. Klajnert, J. Cladera and M. Bryszewska, *Biomacromolecules*, 2006, **7**, 2186–2191.
11 V. Balzani, P. Ceroni, M. Maestri, C. Saudan and V. Vicinelli, *Top. Curr. Chem.*, 2003, **228**, 159–191.
12 G. D. D'Ambruoso and D. V. McGrath, *Adv. Polym. Sci.*, 2008, **214**, 87–147.
13 D.-L. Jiang and T. Aida, *Nature*, 1997, **388**, 454–456.
14 J. M. J. Fréchet, *J. Polym. Sci., Part A: Polym. Chem.*, 2003, **41**, 3713–3725.
15 B. Helms and J. M. J. Fréchet, *Adv. Synth. Catal.*, 2006, **348**, 1125–1148.
16 F. W. Zeng and S. C. Zimmerman, *Chem. Rev.*, 1997, **97**, 1681–1712.
17 D. Astruc, E. Boisselier and C. Ornelas, *Chem. Rev.*, 2010, **110**, 1857–1959.
18 C. Deraedt, N. Pinaud and D. Astruc, *J. Am. Chem. Soc.*, 2014, **136**, 12092–12098.
19 B. J. Boyd, L. M. Kaminskas, P. Karellas, G. Krippner, R. Lessene and C. J. H. Porter, *Mol. Pharmaceutics*, 2006, **3**, 614–627.
20 T. L. Kaneshiro, X. Wang and Z.-R. Lu, *Mol. Pharmaceutics*, 2007, **4**, 759–768.
21 B. W. Greatrex, S. J. Brodie, R. H. Furneaux, S. M. Hook, W. T. McBurney, G. F. Painter, T. Rades and P. M. Rendle, *Tetrahedron*, 2009, **65**, 2939–2950.
22 X. Zhang, K. Luo, G. Wang, Y. Nie, B. He, Y. Wu and Z. Gu, *J. Biomater. Appl.*, 2012, **27**, 17–26.
23 S. Ghosh, M. Dutta, S. Sahu, D. Fujita and A. Bandyopadhyay, *Adv. Funct. Mater.*, 2014, **24**, 1364–1371.
24 J. M. J. Fréchet and D. A. Tomalia, *Dendrimers and Other Dendritic Polymers*, Wiley, New York, 2002.
25 S. Natali and J. Mijovic, *Macromolecules*, 2009, **42**, 6799–6807.
26 J. Duhamel, *Polymers*, 2012, **4**, 211–239.
27 A. D. Meltzer, D. A. Tirrell, A. A. Jones, P. T. Inglefield, D. M. Hedstrand and D. A. Tomalia, *Macromolecules*, 1992, **25**, 4541–4548.
28 D.-L. Jiang and T. Aida, *J. Am. Chem. Soc.*, 1998, **120**, 10895–10901.
29 S. Hecht and J. M. J. Fréchet, *J. Am. Chem. Soc.*, 1999, **121**, 4084–4085.
30 M. Chai, Y. Niu, W. J. Youngs and P. L. Rinaldi, *J. Am. Chem. Soc.*, 2001, **123**, 4670–4678.
31 W. E. Baille, C. Malveau, X. X. Zhu, Y. H. Kim and W. T. Ford, *Macromolecules*, 2003, **36**, 839–847.
32 C. Malveau, W. E. Baille, X. X. Zh and W. T. Ford, *J. Polym. Sci., Part B: Polym. Phys.*, 2003, **41**, 2969–2975.
33 E. Fernandez-Megia, J. Correa and R. Riguera, *Biomacromolecules*, 2006, **7**, 3104–3111.
34 R. Novoa-Carballal, E. Sawen, E. Fernandez-Megia, J. Correa, R. Riguera and G. Widmalm, *Phys. Chem. Chem. Phys.*, 2010, **12**, 6587–6589.
35 D. A. Markelov, V. V. Matveev, P. Ingman, M. N. Nikolaeva, E. Lahderanta, V. A. Shevelev and N. I. Boiko, *J. Phys. Chem. B*, 2010, **114**, 4159–4165.

36 D. A. Markelov, V. V. Matveev, P. Ingman, E. Lahderanta and N. I. Boiko, *J. Chem. Phys.*, 2011, **135**, 124901.
37 L. F. Pinto, J. Correa, M. Martin-Pastor, R. Riguera and E. Fernandez-Megia, *J. Am. Chem. Soc.*, 2013, **135**, 1972–1977.
38 L. F. Pinto, R. Riguera and E. Fernandez-Megia, *J. Am. Chem. Soc.*, 2013, **135**, 11513–11516.
39 R. J. Abraham, J. Fisher and P. Loftus, *Introduction to NMR Spectroscopy*, John Wiley and Sons, New York, 1988.
40 I. M. Neelov, D. A. Markelov, S. G. Falkovich, M. Y. Ilyash, B. M. Okrugin and A. A. Darinskii, *Polym. Sci., Ser. C*, 2013, **55**, 154–161.
41 K. Karatasos, D. Adolf and G. R. Davies, *J. Chem. Phys.*, 2001, **115**, 5310.
42 S. V. Lyulin, A. A. Darinskii, A. V. Lyulin and M. A. J. Michels, *Macromolecules*, 2004, **37**, 4676–4685.
43 Y. Y. Gotlib and D. A. Markelov, *Polym. Sci., Ser. A*, 2007, **49**, 1137–1154.
44 A. Kumar and P. Biswas, *J. Chem. Phys.*, 2011, **134**, 214901.
45 A. Kumar and P. Biswas, *Phys. Chem. Chem. Phys.*, 2013, **15**, 20294–20302.
46 D. A. Markelov, S. V. Lyulin, Y. Y. Gotlib, A. V. Lyulin, V. V. Matveev, E. Lahderanta and A. A. Darinskii, *J. Chem. Phys.*, 2009, **130**, 044907.
47 D. A. Markelov, M. Dolgushev, Y. Y. Gotlib and A. Blumen, *J. Chem. Phys.*, 2014, **140**, 244904.
48 M. Dolgushev and A. Blumen, *Macromolecules*, 2009, **42**, 5378–5387.
49 M. Dolgushev and A. Blumen, *J. Chem. Phys.*, 2009, **131**, 044905.
50 F. Fürstenberg, M. Dolgushev and A. Blumen, *J. Chem. Phys.*, 2012, **136**, 154904.
51 S. Falkovich, D. Markelov, I. Neelov and A. Darinskii, *J. Chem. Phys.*, 2013, **139**, 064903.
52 W. L. Jorgensen, J. Chandrasekhar, J. D. Madura, R. W. Impey and M. L. Klein, *J. Chem. Phys.*, 1983, **88**, 2472.
53 E. J. Sorin and V. S. Pande, *Biophys. J.*, 2005, **88**, 2472–2493.
54 B. Hess, C. Kutzner, D. van der Spoel and E. Lindahl, *J. Chem. Theory Comput.*, 2008, **4**, 435–447.
55 (*a*) G. P. Vlasov, V. I. Korol'kov, G. A. Pankova, I. I. Tarasenko, A. N. Baranov, P. B. Glazkov, A. V. Kiselev, O. V. Ostapenko, E. A. Lesina and V. S. Baranov, *Russ. J. Bioorg. Chem.*, 2004, **30**, 12–20; (*b*) G. P. Vlasov, G. M. Pavlov, N. V. Bayanova, E. V. Korneeva, C. Ebel, M. A. Khodorkovskii and T. O. Artamonova, *Dokl. Phys. Chem.*, 2004, **399**, 290–292.
56 B. P. Roberts, G. Y. Krippner, M. J. Scanlon and D. K. Chalmers, *Macromolecules*, 2009, **42**, 2784–2794.
57 V. I. Chizhik, Y. S. Chernyshev, V. V. Frolov, A. V. Komolkin and M. A. Shelyapina, *Magnetic Resonance and Its Applications*, Springer, Cham, 2014.
58 Y. Y. Gotlib, I. M. Neelov and I. A. Torchinskii, *Macromol. Theory Simul.*, 1993, **2**, 1–11.